Supporting Information

Local transport measurements in Graphene on SiO_2 using Kelvin Probe Force Microscopy

Philip Willke[1], Christian Möhle[1], Anna Sinterhauf[1], Thomas Kotzott[1], Hak Ki Yu[2,3,4], Alec Wodtke[2,3], Martin Wenderoth[1,]*

1 IV. Physical Institute, University of Göttingen, 37077 Göttingen, Germany

2 Institute for Physical Chemistry, University of Göttingen, 37077 Göttingen, Germany

3 Max Planck Institute for Biophysical Chemistry, 37077 Göttingen, Germany

4 Department of Materials Science & Engineering, Ajou University, Suwon 443-749, Korea

*To whom correspondence should be addressed: E-mail: mwender@gwdg.de (M.W.)

1. Resistor network simulations and current inhomogeneities

In the data analysis we assume a homogeneous current density j_{macro} over the sample. To estimate the homogeneity of the current distribution we perform classical resistor network simulations of the transport map as introduced by Homoth *et al.*[1]. The sample system has been modelled corresponding to the topography in Figure 2a by connecting the data points with resistors horizontally and vertically. The area is divided into monolayer, bilayer, and wrinkle areas and to each resistor the value of the experimental results as given in the manuscript is assigned. The potential $V_{Transport}$ on the left and right image borders is derived by a linear fit of the experimental transport data. The result of the simulated potential map is shown in Figure S1a. It is highly dominated by a linear voltage drop. From potential and resistance values the local current in each data point can be calculated. The current map can be found in Figure S1b. The edges of defects, i.e. ML/BL steps and wrinkles, are sketched by black lines because the simulation of the currents in these edges depends on the discretization of the model. However, the current flow on free areas is consistently described for the given surface structure including defects. The current density is found to be homogeneous over the 30µm x 30µm sample as depicted in Figure S1c. Both, a Gaussian fit and statistical evaluation of the data, give a coefficient of variation, i.e. a ratio of standard deviation to the mean value of $\sigma/\mu = 3.8\%$ over the whole area for the resistance values from the manuscript $\rho_{ML} = 342\ \Omega$, $\rho_{ML/BL} = 20\ \Omega\mu m$, and $\rho_{Wr} = 50\ \Omega\mu m$. Hence, the simulation justifies the assumption of a nearly homogeneous current density. An uncertainty of 4% is included in the calculation of the error of sheet and wrinkle resistances.

Even for an increased wrinkle resistance of $\rho_{Wr} = 200\ \Omega\mu m$, the standard deviation of the current is still given by a value of 6%. However, then the voltage drop over the wrinkle should

be in the order of $\Delta V \approx 8\text{mV}$ for a current density of $j_{\text{macro}} = 39\ \frac{\text{A}}{\text{m}}$ which is substantially above the experimental results (see Figure 4d).

On the nanoscale the orientation of the current in the free graphene sheet is to very high extent given by the horizontal component, i.e. parallel to the macroscopic current density. Therefore it is legitimate for the evaluation of wrinkle resistances to assume the microscopic current to be running horizontally with the macroscopic current density.

As shown in Figure 2h in the manuscript, the sheet resistances for different areas vary by up to 8%. We found that even including such variations in the simulations by applying a Gaussian to the resistance values on free areas does not change the uniformity of the current significantly and results in a still moderate coefficient of variation of 6%.

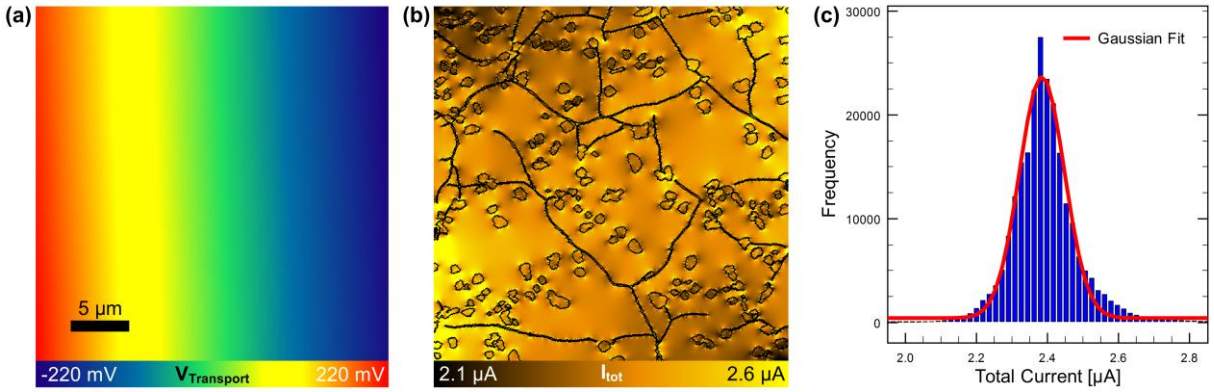

Figure S1. Resistor network simulation of the transport map shown as Figure 2e in the manuscript with a discretization of 512x512 data points matching the KPFM resolution. (a) Transport potential $V_{\text{Transport}}$ resulting from a network with resistor values $\rho_{\text{ML}} = 342\ \Omega$, $\rho_{\text{ML/BL}} = 20\ \Omega\mu\text{m}$, and $\rho_{\text{Wr}} = 50\ \Omega\mu\text{m}$. (b) Local current map with defects sketched in black. (c) Histogram of total currents of the map shown in (b) with Gaussian fit with mean value $\mu = 2.38\mu\text{A}$ and standard deviation $\sigma = 8.95 \cdot 10^{-2}\mu\text{A}$. The relative deviation of $\sigma/\mu = 3.8\%$ shows the homogeneity of the current density over the sample.

2. Modelling the temperature-dependence of graphene on SiO_2

The temperature-dependence of graphene on SiO_2 has been discussed by Chen *et al.*[2] As described in the manuscript, the additional dependence has been introduced by a linear temperature-dependence $\rho_A(T)$ due to acoustic phonons and an exponential contribution due to

coupling to phonon-modes in the substrate. In the simplest model this has been expressed as a single contribution.[2] A third contribution ρ_0 is independent of temperature and thus limits the low-temperature case. Thus, the dependence is given by

$$\rho(T) = \rho_0 + \rho_A(T) + \rho_B(T) \tag{S1}$$

with $\rho_A(T) = K_1 \cdot T = \left(\frac{h}{e^2}\right) \frac{\pi^2 D_A^2 k_B}{2h^2 \rho_s v_S^2 v_F} \cdot T$ and $\rho_B(T) = K_2 \cdot \left(\frac{1}{e^{E_0/k_B T} - 1}\right)$

Here, D_A is the acoustic deformation potential, ρ_s is the 2D mass density of graphene, v_s is the velocity for LA phonons and v_F is the Fermi-velocity. Using the values in [2] we set $K_1 = 0.0316 \frac{1}{K}$. Moreover, K_2 has been introduced to take account for the dependence on the gate voltage. Therefore, we also replace it with the value for no gate voltage $K_2 = 5730\ \Omega$, as in our experiment. Our best fit parameters for the macroscopic case and the two local dependencies can be found in Table S1.

	$\boldsymbol{\rho_0}$ **[Ω]**	$\mathbf{E_0}$ **[meV]**
$\boldsymbol{\rho_{macro}}$	303	122
$\boldsymbol{\rho_{ML,1}}$	260	129
$\boldsymbol{\rho_{ML,2}}$	298	127

Table S1. Parameters to describe the temperature-dependent resistance.

3. Resistor network model for a folded graphene wrinkle

The concepts of the resistor network model have been introduced elsewhere.[1,3] Figure S2 depicts the equivalent circuit diagram of the resistor network model for the folded graphene wrinkle. $R_{ML} = \frac{W}{L} \cdot \rho_{ML}$ is here the resistance of a segment of monolayer graphene (sheet

resistance $\rho_{ML} = 350\ \Omega$) with length L and width W. We here neglected any possible changes in the charge carrier concentration of the single layers and assumed an equal distribution, so that all three layers have the same resistance. Additionally, interlayer resistance $R_{\perp,12}=\kappa \cdot R_{ML} \cdot \frac{d^2}{W \cdot L}$ can be expressed as a multiple κ of the ML resistance R_{ML} (times the dimensionless factor $\frac{d^2}{W \cdot L}$ with $d = 3.4\ \text{Å}$ the graphite layer thickness, that accounts for the different current direction). While L and W are introduced here to define the values of the resistance, the results are independent of them as long as the choice of the grid is made small enough.

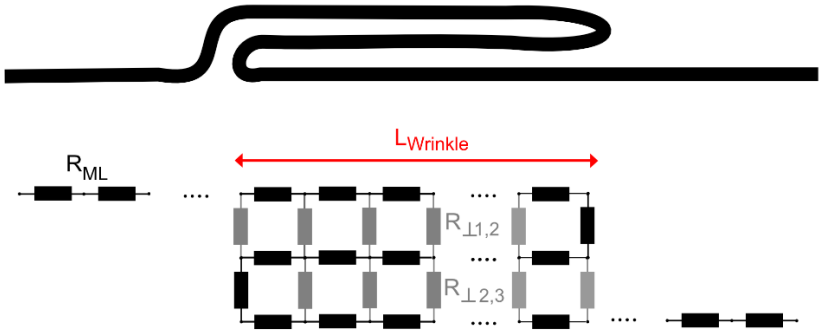

Figure 2. Geometry and equivalent circuit diagram of the folded graphene wrinkle.

We use κ as a fitting factor to the experimental data. $R_{\perp,12}$ and $R_{\perp,23}$ are the interlayer resistances for the first and second/second and third layer, respectively. We now simulate two limiting cases

1. $R_{\perp,12} \ll R_{\perp,23}$: This implicates that the folded wrinkle is only coupled to the upper (or lower) sheet as has been assumed in [4].
2. $R_{\perp,12} = R_{\perp,23}$: This is the case when the wrinkle couples to both sheets and forms a trilayer-like structure as suggested by the KPFM data in the manuscript.

The evaluation of the defect resistance $\rho_{Wrinkle}$ is performed analogously to the experimental data in the manuscript by fitting linear functions to the regions left and right of the defect and

dividing the voltage drop by the current density. Figure S3a depicts the result for case 1 and Figure S3b for case 2. We show the defect resistance as a function of the wrinkle length $L_{Wrinkle}$ as well as for different values κ. For case 1, two regimes can be distinguished: for small values of $L_{Wrinkle}$ the increase is linear, since the wrinkle is too short for electrons to tunnel between the layers and thus the transport is still dominated by the in-plane transport. For larger values of $L_{Wrinkle}$ the resistance saturates, since now the transport is completely dominated by tunneling and thus independent of the length of the wrinkle. This is in agreement with the simulation by Zhu *et al*.[4] The gray area marks the range of $L_{Wrinkle}$ observed experimentally. Consequently, here the transport is already dominated by the tunneling. For case 2, the transport is even decreasing for long wrinkles, since the transport can take place in all three layers effectively reducing the resistance in the wrinkle (even leading to lower resistances than on the ML). The experimentally observed defect resistance is $\rho_{Wrinkle} \approx 50\ \Omega\mu m$. Thus, we obtain the best fit with $\kappa = 1 \cdot 10^5$ (case 1) and $\kappa = 4 \cdot 10^5$ (case 2). The resistance between two layers can also be treated as a contact resistance[2] that can be calculated by

$$R_C = \frac{1}{2} \cdot \kappa \cdot \rho_{ML} \cdot d^2 \qquad \text{(S2)}$$

Leading to

$R_{C,1}=2\cdot10^{-8}\Omega cm^2$ (case 1) $R_{C,2}=8\cdot10^{-8}\Omega cm^2$ (case 2)

As stated in the manuscript, this is significantly higher than the contact resistance found for the monolayer bilayer transition in epitaxial graphene ($4.2\cdot10^{-10}\Omega cm^2$).[2] This can be explained with a weaker coupling than in epitaxial graphene. In fact, since the atomic lattice is not resolved in this experiment, we cannot determine the stacking of the different layers. This should however be crucial for the interlayer tunneling.

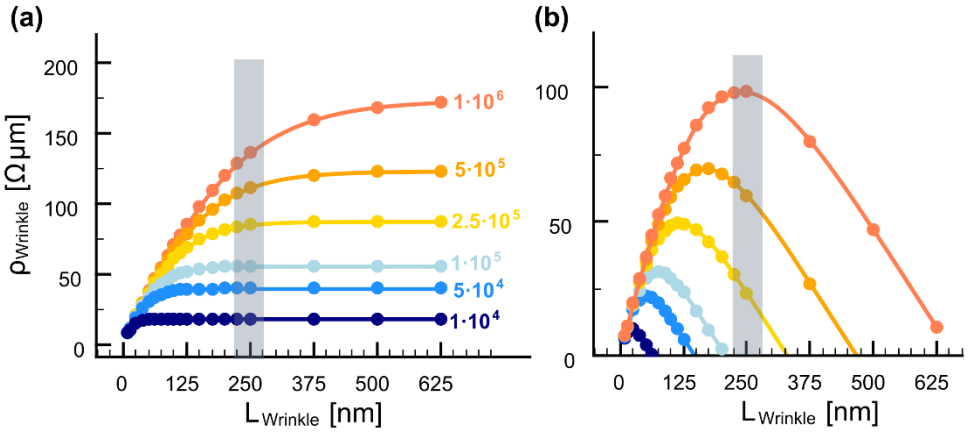

Figure S3. Results for the resistor network model of the folded graphene wrinkle with the defect resistance $\rho_{Wrinkle}$ as a function of wrinkle length $L_{Wrinkle}$. (a) Results for a bilayer coupling ($R_{\perp,12} \ll R_{\perp,23}$) for different values of κ between 10^4 and 10^6. (b) Results for trilayer coupling ($R_{\perp,12} = R_{\perp,23}$) for different values of κ between 10^4 and 10^6 [same as in (a)]. Gray area marks the experimentally investigated length of folded graphene wrinkles.

4. Temperature-dependence of the step resistance of folded bilayer wrinkles

In Figure S4 we show the data from Figure 4d in the manuscript, now explicitly the step resistance of the folded graphene wrinkle $\rho_{Wrinkle}$ as a function of temperature T. This is calculated by

$$\rho_{Wrinkle} = \frac{\Delta V}{j_{macro}} \tag{S3}$$

and the measured relation between the temperature and the current density is given by $T=(0.0089\pm0.0002)\,\frac{m^2}{A^2}\,K\cdot j_{macro}^2+(298.9\pm0.7)K$. Note that the current-dependence of Equation S3 is due to temperature-independent reasons, namely the dependence on the sample width and the applied bias voltage V_{Bias}. We now fitted two models to the data points, the temperature-independent case

$$\rho_{Wrinkle}(T) = \rho_0 \cdot l_{eff} \tag{S4}$$

and a model for the temperature-dependent behavior as observed on the ML sheets

$$\rho_{Wrinkle}(T) = [\rho_0 + \rho_A(T) + \rho_B(T)] \cdot l_{eff} \quad \text{(S5)}$$

Here, we also introduced the effective length l_{eff} that corresponds to the length of a graphene channel that would yield the same resistance as the defect. This concept has been used previously to describe localized defects[5,6] and is introduced here to relate the defect resistance $\rho_{Wrinkle}$ ([Ωm]) to the sheet resistance ρ_{ML} ([Ω]). We use $l_{eff} = 0.15$ µm so that the temperature-independent resistance ρ_0 is close to the measured sheet resistance $\rho_{ML} \approx 350$ Ω. In both models we use ρ_0 as the only fitting parameter. For the temperature-dependent case we use the same values for the parameters K_1, K_2 and E_0 as for the ML sheet resistance ρ_{ML} (see Supplementary Information, Section 2). Note that the influence of the temperature-dependent part can be scaled by other choices of l_{eff}. The choices made here assume the same relative increase in the given temperature-range as for the monolayer sheet resistance ρ_{ML}. This would for example be the case, if the transport through the wrinkle is simply given by the elongated path in case of no interlayer tunneling (see Supplementary Information, Section 3). The best fits to the data for the T-independent case and for the T-dependent case are shown in Figure S4 as orange and black line, respectively.

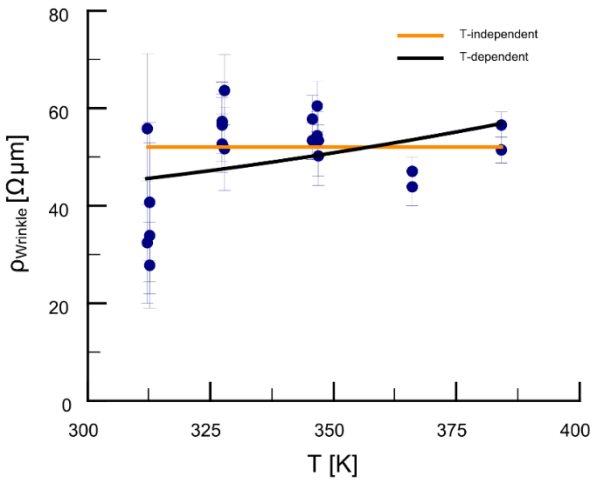

Figure S4. Step resistance $\rho_{Wrinkle}$ of the folded graphene wrinkle shown in Figure 4 in the manuscript as a function of temperature T. Orange line indicates the fit to the temperature-independent model. The black line corresponds to the temperature-dependent model with an increase in resistance as observed on the graphene sheets.

While both lines seem to describe the data equally well, a more detailed statistical analysis reveals the differences in the quality of the fits. By comparing the chi-squared

$$\chi^2 = \sum_{i=1}^{N} \left(\frac{\rho_i - \rho(T_i)}{\sigma_i} \right) \tag{S6}$$

with the error $\sigma_{\rho_{Wrinkle}}$ of the wrinkle defect resistance we find a 30% higher value for the T-dependent model than for the T-independent case.

$$\frac{\chi^2_{\text{T-dependent}}}{\chi^2_{\text{T-independent}}} = 130\ \%$$

In fact, this is even more pronounced when we exclude the data points at $T = 312$ K. As can be seen from Figure 4d in the manuscript the total voltage drop ΔV is very small and close to the noise limit. This leads to high errors, since $\sigma_{\rho_{Wrinkle}} = \frac{\sigma_{\Delta V}}{\Delta V} \cdot \rho$. While these points cannot be described well by any of the two models, they are the only ones motivating a positive slope as required for the T-dependent model. Thus, excluding the data at $T = 312$ K from the statistical analysis even leads to

$$\frac{\chi^2_{\text{T-dependent}}}{\chi^2_{\text{T-independent}}} = 193\ \%$$

So almost twice as high for the T-dependent case. This even holds for different choices for the effective length l_{eff}. As discussed above, this effectively scales the influence of the temperature-dependent part of the resistance. In Figure S5a we show the dependence of χ^2 on l_{eff} for both models. As can be seen, for all choices of l_{eff}, we find that χ^2 is higher for the temperature-dependent model. For small values of l_{eff}, the temperature-dependent data converges to the temperature-independent case. However, in this limit the temperature-dependence is so small that it hardly differs from the independent model as can be seen in Figure S5b.

Consequently, if the wrinkle resistance $\rho_{Wrinkle}$ was temperature-dependent, our data suggests that this dependence would be smaller than the ML sheet resistance, while the best fit is obtained with a temperature-independent model. Thus, we hypothesize that the step resistance $\rho_{Wrinkle}$ at the folded graphene wrinkle does not change with temperature.

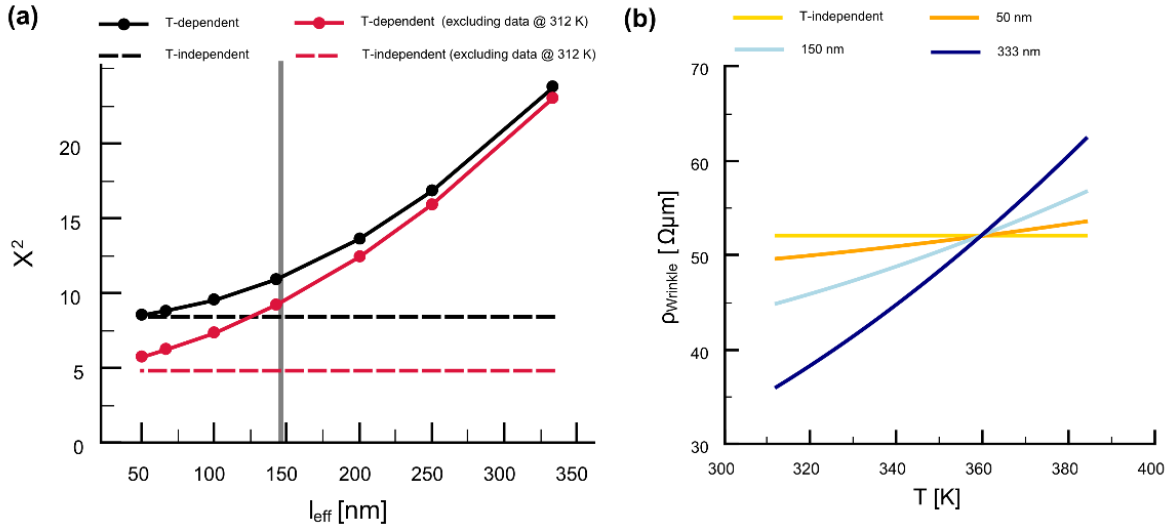

Figure S5. (a) Chi-squared χ^2 as a function of effective length l_{eff} for all data points (black) and for excluding the lowest data points at T = 312 K (red). The continuous (dashed) lines show the results for the temperature-dependent (temperature-independent) model. Grey line indicates the choice of l_{eff} for the same temperature-dependence as for the ML sheet resistances. (b) Wrinkle resistance $\rho_{Wrinkle}$ as a function of temperature T for different values of l_{eff}.

REFERENCES

(1) Homoth, J.; Wenderoth, M.; Druga, T.; Winking, L.; Ulbrich, R. G.; Bobisch, C. A.; Weyers B.; Bannani A.; Zubkov E.; Bernhart A. M.; Kaspers M. R.; Moller, R.; Electronic transport on the nanoscale: ballistic transmission and Ohm's law. *Nano Lett.*, **2009**, *9*, 1588-1592. DOI: 10.1021/nl803783g

(2) Chen, J. H.; Jang, C.; Xiao, S.; Ishigami, M.; Fuhrer, M. S. Intrinsic and extrinsic performance limits of graphene devices on SiO2. *Nat. Nanotechnol.* **2008**. *3*, 206-209.

(3) Willke, P.; Druga, T.; Ulbrich, R. G.; Schneider, M. A.; Wenderoth, M. Spatial extent of a Landauer residual-resistivity dipole in graphene quantified by scanning tunnelling potentiometry. *Nat. Commun.* **2015**, *6,* 6399. DOI: 10.1038/ncomms7399

(4) Zhu, W.; Low, T.; Perebeinos, V.; Bol, A. A.; Zhu, Y.; Yan, H.; Tersoff, J.; Avouris, P. Structure and Electronic Transport in Graphene Wrinkles. *Nano Lett.* **2012**, *12*, 3431–3436. DOI: 10.1021/nl300563h

(5) Grosse, K. L.; Dorgan, V. E.; Estrada, D.; Wood, J. D.; Vlassiouk, I.; Eres, G.; Lyding, J. W.; King, W. P.; Pop, E. Direct observation of resistive heating at graphene wrinkles and grain boundaries. *Appl. Phys. Lett.* **2014** *105*, 143109. DOI: 10.1063/1.4896676

(6) Yu, Q.; Jauregui, L. A.; Wu, W.; Colby, R.; Tian, J.; Su, Z.; Cao, H.; Liu, Z.; Pandey, D.; Wei, D.; et al. Control and Characterization of Individual Grains and Grain Boundaries in Graphene Grown by Chemical Vapour Deposition. *Nat. Mater.* **2011**, *10*, 443–449. DOI: 10.1038/nmat3010